Quaternary volcano-tectonic activity in the Soddo region, western margin of the Southern Main Ethiopian Rift

Giacomo Corti,[1] Federico Sani,[2] Melody Philippon,[3] Dimitrios Sokoutis,[3,4] Ernst Willingshofer,[3] and Paola Molin[5]

Received 20 March 2013; revised 14 May 2013; accepted 21 May 2013; published 1 July 2013.

[1] We present an analysis of the distribution, timing, and characteristics of the volcano-tectonic activity on the western margin of the Southern Main Ethiopian Rift in the Soddo area (latitudes between ~7°10'N and ~6°30'N). The margin is characterized by the presence of numerous normal faults, with limited vertical offset and often sigmoidal in shape, which accommodate a gentle transition from the rift floor to the Ethiopian plateau. New radiocarbon dating indicates post-30 ka fault activity, pointing to a significant Late Pleistocene-Holocene tectonic activity of the Soddo margin. Comparison of the fault architecture with analog models suggests that deformation has been controlled by a sub-E-W (roughly N100°E) extension direction, resulting in an oblique extension with respect to the roughly NE-SW-trending rift. This well accords with inversion of fault slip data collected on faults with Pleistocene-Holocene activity and is also in good agreement with recent GPS data from the Southern Main Ethiopian Rift. Our data support a close correlation between the recent volcanic activity and deformation in the study area, with eruptive vents located along the recent border faults; the axial tectono-magmatic activity is subordinate in the area. These findings support a transition from axial tectono-magmatic deformation in the Northern Main Ethiopian Rift to marginal deformation in the Central and Southern Main Ethiopian Rift, in turn indicating an along-axis, north to south decrease in rift maturity.

Citation: Corti, G., F. Sani, M. Philippon, D. Sokoutis, E. Willingshofer, and P. Molin (2013), Quaternary volcano-tectonic activity in the Soddo region, western margin of the Southern Main Ethiopian Rift, *Tectonics*, *32*, 861–879, doi:10.1002/tect.20052.

1. Introduction

[2] Defining the distribution, style, and timing of deformation and its relations with volcanic events during progressive extension of the continental lithosphere is crucial in understanding the dynamics by which continental plates are split apart and how faulting and magmatism relatively contribute to continental rifting and breakup [e.g., *Ebinger*, 2005]. The Main Ethiopian Rift (MER) in East Africa (Figure 1) is considered the ideal place to analyze these processes. In fact, the along-axis variations of rift-related deformation that characterize the different MER sectors (Northern MER, Central MER, and Southern MER) have been typically interpreted as reflecting a variation in rift evolution from mature rifting in the Northern MER to less evolved rifting southward [e.g., *Hayward and Ebinger*, 1996; *Corti*, 2009; *Agostini et al.*, 2011a]. Analysis of fault distribution, field geological investigations, and comparison with analog models, together with the characteristics of the seismic activity, support an incipient breakup stage in the Northern MER, with abandoned boundary faults and focused tectono-magmatic activity at the rift axis [e.g., *Wolfenden et al.*, 2004; *Keir et al.*, 2006; *Agostini et al.*, 2011a]; geophysical data further support these observations and indicate an important magmatic modification of the crust in this area [e.g., *Keranen and Klemperer*, 2008]. Similar analysis in the Central MER indicates instead a less advanced rifting stage, with a significant part of deformation localized at large boundary faults and axial deformation in an incipient stage only [e.g., *Agostini et al.*, 2011a, 2011b]; volcanism and magmatic modification of the crust/lithosphere are comparatively less developed in this region [e.g., *Keranen and Klemperer*, 2008]. Comparison of analog models with an analysis of fault distribution [*Agostini et al.*, 2011a] suggests a further decrease in rift evolution in the Southern MER, with marginal deformation and absent axial faulting, indicating an early stage of extension. This conclusion is supported by analysis of the overall rift morphology [*Hayward and Ebinger*, 1996], as well as the distribution of earthquakes in the area, with main shocks always related to deformation at the rift margins [*Keir et al.*, 2006]. However, geological data are currently still scattered

Additional supporting information may be found in the online version of this article.

[1]Istituto di Geoscienze e Georisorse, Consiglio Nazionale delle Ricerche, Florence, Italy.
[2]Dipartimento di Scienze della Terra, Università degli Studi di Firenze, Florence, Italy.
[3]Department of Tectonics, Faculty of Earth Sciences, Utrecht University, Utrecht, The Netherlands.
[4]Department of Geosciences, University of Oslo, Oslo, Norway.
[5]Dipartimento di Scienze, Università degli Studi di Roma Tre, Rome, Italy.

Corresponding author: G. Corti, Istituto di Geoscienze e Georisorse, Consiglio Nazionale delle Ricerche, Via G. La Pira, 4, IT-50121 Florence, Italy. (giacomo.corti@unifi.it)

0278-7407/13/10.1002/tect.20052

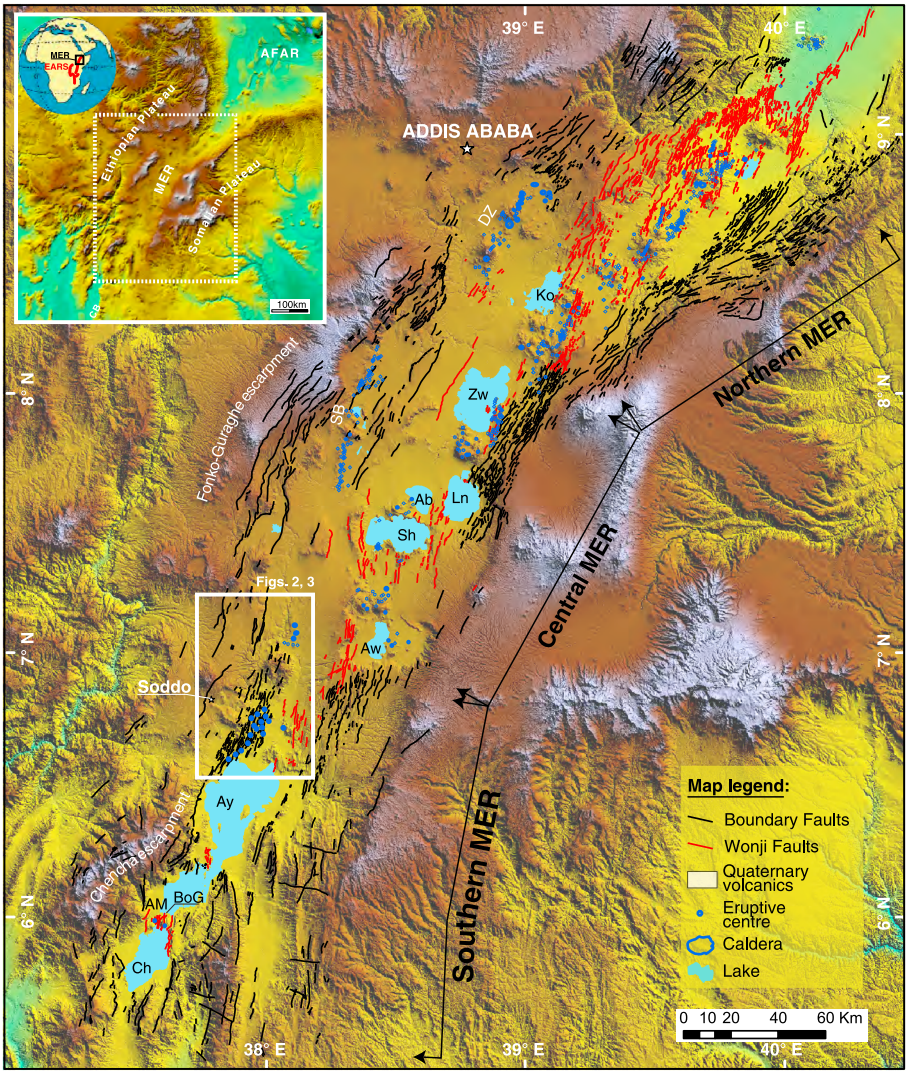

Figure 1. Fault pattern of the Main Ethiopian Rift (MER) (modified from *Agostini et al*. [2011a]) superimposed on a digital elevation model (Shuttle Radar Topography Mission, SRTM data), indicating the three main rift sectors (Northern, Central, and Southern MER). Inset shows the location of the MER within the East African Rift (EARS). Ab: Lake Abijata; AM: Arba Minch; Ay: Lake Abaya; Aw: Lake Awasa; BoG: Bridge of God; Ch: Lake Chamo; DZ: Debre Zeyt volcanic field; Ko: Lake Koka; Ln: Lake Langano; SB: Silti-Butajira volcanic field; Sh: Lake Shala; Zw: Lake Ziway.

in the Southern MER, and knowledge of the distribution and style of Quaternary volcano-tectonic deformation is comparatively less constrained than in the other MER sectors. In this contribution, we aim at filling this gap, by presenting new geological data on the western margin of the Southern MER in the Soddo area (latitudes between ~7°10'N and ~6°30'N; Figure 1). In particular, we present new field structural data coupled with C14 radiometric dating of faulted rocks that shed new light on the distribution, timing, and characteristics of Quaternary deformation and its relations with the extensive volcanism that characterizes this rift sector. These new data, implemented with a geomorphic analysis of the local hydrographic pattern, support an important Late Quaternary-Holocene volcano-tectonic activity at the rift margin. Together with a decrease in the volumes of rift-related volcanic products and a subordinate axial faulting, these findings support previous models that predict an along-axis, north to south decrease in rift maturity in the MER [e.g., *Hayward and Ebinger*, 1996].

2. Regional Setting

[3] The MER is located at the northern termination of the East African Rift System (EARS) and extends from the Afar triple junction in the north, to the Turkana Rift in the south (Figure 1a). The MER is traditionally differentiated into three main sectors (Northern MER, Central MER, and Southern MER) differing in terms of rift trend, fault timing and patterns, and lithospheric characteristics (Figure 1) [e.g., *Mohr*, 1983; *Hayward and Ebinger*, 1996; *Bonini et al*., 2005; *Corti*, 2009]. The Northern MER shows two well-developed fault systems: (1) a set of roughly NE-SW-trending border faults and (2) a set of roughly NNE-SSW-trending faults affecting the rift floor, usually referred to as Wonji

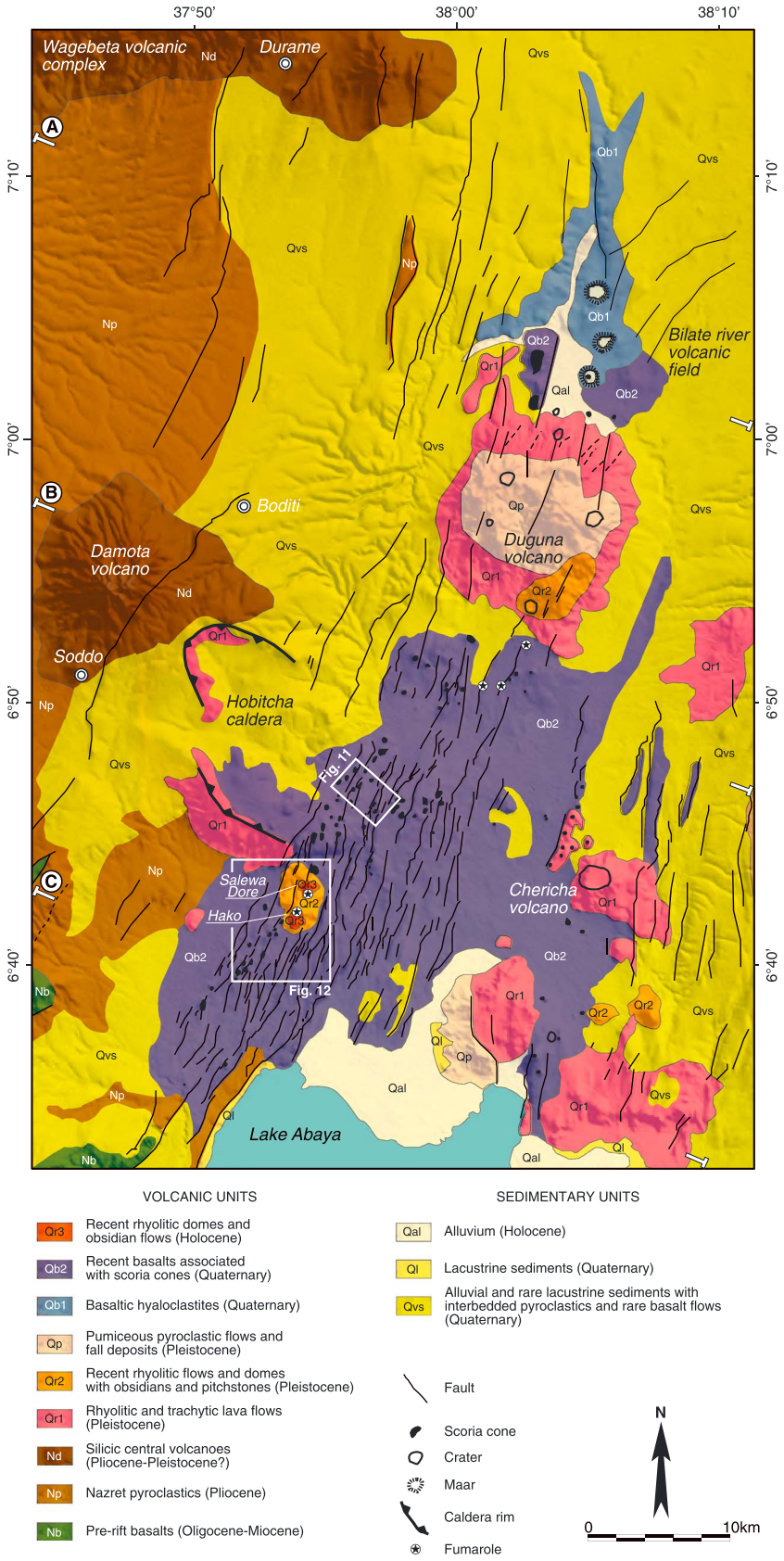

Figure 2. Geological map of the Soddo area (modified from *Ethiopian Mapping Agency* [1981] *Chernet* [2011]). Indicated is the location of the three cross sections (A, B, and C) illustrated in Figure 6.

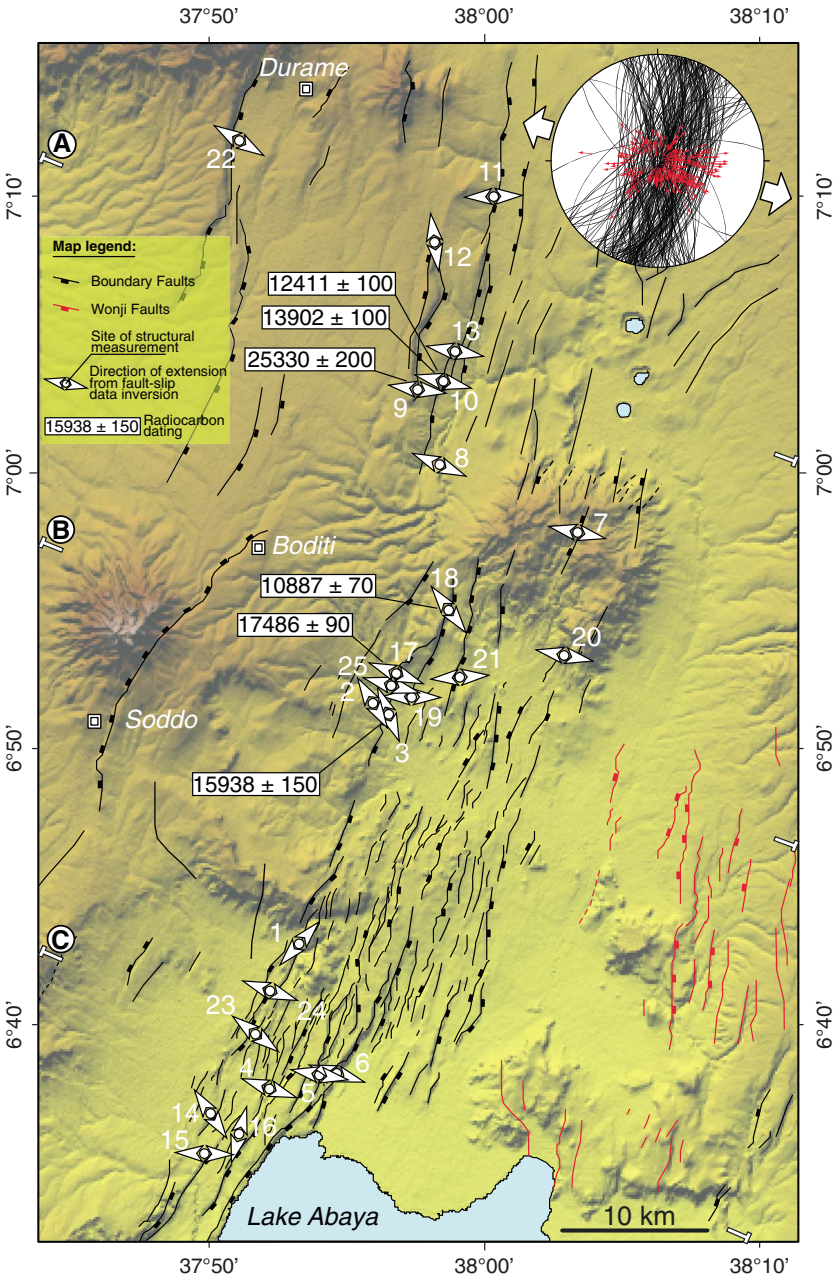

Figure 3. Structural map of the Soddo area with sites of structural measurements (numbers as in Table 1) and directions of extension obtained through fault slip data inversion. Indicated is the location of the three cross sections (A, B, and C) illustrated in Figure 6. Top-right plot displays the cumulative analysis of fault slip data (Wulff net, lower hemisphere) collected in the Soddo area. All paleostress determinations have been obtained using the dihedron angles method of *Angelier and Mecheler* [1977].

Fault Belt (WFB) [e.g., *Mohr*, 1962, 1967; *Gibson*, 1969; *Boccaletti et al.*, 1998]. The long, large-offset border faults are interpreted to have accommodated the tectonic deformation during the initial, Mio-Pliocene (post-11 Ma) stages of rifting [*Hayward and Ebinger*, 1996; *Boccaletti et al.*, 1998] but are suggested to have been deactivated and mostly eroded during the Pleistocene [*Wolfenden et al.*, 2004; *Casey et al.*, 2006; *Keir et al.*, 2006]. Recent and active deformation is indeed believed to be accommodated by the WFB, an axial tectono-volcanic system characterized by swarms of short, closely spaced faults with minor vertical throw, with associated focused strong bimodal volcanic activity and magma intrusion [e.g., *Boccaletti et al.*, 1999; *Ebinger and Casey*, 2001]. Strong relations between the architecture and characteristics of the WFB and voluminous middle-to-lower crustal magma intrusion have been highlighted by geophysical data, which point to a strong tectono-magmatic modification of the crust and lithosphere beneath the WFB segments [e.g., *Keir et al.*, 2006; *Keranen and Klemperer*, 2008]. Analysis of instrumental seismicity [*Keir et al.*, 2006], Late Quaternary-recent volcanic activity [*Rooney et al.*, 2007], and geodetic measurements [*Billham et al.*, 1999; *Bendick*

Table 1. Inversion of Fault Slip Data Collected in the Study Area[a]

Site Number	Number of Data	Latitude	Longitude	Age of Youngest Deformed Rock	σ1		σ2		σ3	
					Dip Dir.	Dip	Dip Dir.	Dip	Dip Dir.	Dip
1	7	6°42'52.60"N	37°53'17.30"E	Quaternary	339	70	129	17	222	9
2	12	6°51'53.30"N	37°56'28.70"E	Pleistocene	217	80	59	10	329	4
3	11	6°51'47.40"N	37°56'30.40"E	Pleistocene[b]	56	87	248	3	158	1
4	5	6°37'34.90"N	37°52'01.40"E	Quaternary	300	48	204	6	109	42
5	7	6°37'46.60"N	37°53'52.70"E	Quaternary	279	80	10	0	100	10
6	12	6°38'01.90"N	37°54'30.40"E	Quaternary	339	83	198	5	107	4
7	5	6°58'05.90"N	38°03'36.80"E	Pleistocene	109	74	12	2	282	15
8	20	6°59'34.00"N	37°58'36.00"E	Pleistocene	357	84	203	6	113	3
9	11	7°02'42.63"N	37°57'17.10"E	Pleistocene[b]	251	82	8	4	98	7
10	10	7°03'09.10"N	37°58'24.00"E	Pleistocene[b]	166	76	14	12	283	6
11	8	7°09'59.00"N	38°00'15.20"E	Pleistocene	276	59	180	4	88	31
12	4	7°08'39.10"N	37°58'09.10"E	Pleistocene	245	60	87	28	352	9
13	5	7°04'22.30"N	37°59'14.20"E	Pleistocene	282	55	191	1	100	35
14	7	6°36'33.90"N	37°50'01.40"E	Quaternary	275	63	50	19	146	18
15	12	6°35'29.50"N	37°50'12.30"E	Quaternary	254	60	358	8	92	29
16	3	6°35'56.80"N	37°51'07.70"E	Quaternary	81	48	300	35	195	20
17	10	6°52'40.40"N	37°56'43.80"E	Pleistocene[b]	202	3	300	69	11	20
18	10	6°54'27.00"N	37°58'24.50"E	Pleistocene[b]	50	11	281	72	143	14
19	7	6°51'44.00"N	37°57'06.60"E	Pleistocene	7	44	175	45	271	6
20	2	6°52'09.00"N	38°03'46.10"E	Pleistocene	1	17	245	56	101	29
21	2	6°52'06.80"N	37°58'54.10"E	Pleistocene	183	9	285	51	86	38
22	13	7°12'54.60"N	37°50'45.30"E	Pleistocene	209	70	31	20	301	1
23	7	6°39'16.00"N	37°51'14.00"E	Pleistocene	127	67	31	2	300	23
24	5	6°41'10.03"N	37°51'57.43"E	Pleistocene	109	52	4	11	266	353
25	15	6°52'06.61"N	37°56'38.67"E	Pleistocene	310	84	194	2	103	10

[a][Paleostress Orientation Calculated From the Dihedron Angles Method by *Angelier and Mecheler*, 1977].
[b]Faulted debris dated; see Table 2.

et al., 2006] support that plate separation is almost entirely accommodated within the WFB segments, through a phase of magma-assisted rifting that characterize the late stages of continental rifting [e.g., *Kendall et al*., 2005; *Bastow et al*., 2010].

[4] In the Central MER, Late Miocene-Pliocene boundary faults (post-6-7 Ma) are well developed, and analysis of historical seismicity [*Gouin*, 1979; *Keir et al*., 2006] and geological data [*Pizzi et al*., 2006; *Agostini et al*., 2011b] suggest these faults to be characterized by significant Quaternary deformation. Radiocarbon dating of faulted material [*Agostini et al*., 2011b] indicates a Late Pleistocene-Holocene (post-30 ka) fault activity at large offset boundary faults at both rift margins. Geophysical data in the Central MER are less abundant than in the Northern MER, but the available information supports a decrease in the tectono-magmatic modification of the crust and lithosphere proceeding from the Northern MER sector southward [e.g., *Keranen and Klemperer*, 2008]. However, two different subparallel belts of focused tectonic-magmatic activity characterize both rift margins of the Central MER [e.g., *Woldegabriel et al*., 1990; *Rooney et al*., 2007, 2011]: the WFB is mostly localized close to the eastern margin, whereas a volcanic belt extending between Silti-Butajira and Debre Zeyt characterizes the western margin (Figure 1). Notably, whereas intense faulting and a well-developed magma plumbing system characterize the WFB, the Silti-Butajira-Debre Zeyt belt lacks significant surface faulting and is associated to a less evolved magmatic system [e.g., *Rooney et al*., 2007, 2011; *Rooney*, 2010]. This difference has been interpreted as reflecting more pronounced extension and thinning within the WFB at the eastern margin of Central MER [*Rooney*, 2010]. The lack of significant faulting and volcanism in the center of the rift floor suggests that axial tectonic and magmatic deformation is subordinate in the area [*Agostini et al*., 2011b].

[5] In the Southern MER, extensional basins are bounded by faulted escarpments characterized by large-offset, major

Table 2. Radiometric Age Determinations of the Faulted Debris Smeared Along the Fault Plane[a]

Site	Laboratory Code	Locality	Latitude	Longitude	Lithology	Radiocarbon Age	Calibrated Age (2σ)
Site 3	LTL8059A	Bedessa	6°51'46.30"N	37°56'32.30"E	Debris[b]	15,938 ± 150	
Site 9	LTL12217A	North of Duguna	7°2'42.63"N	37°57'17.10"E	Debris[b]	25,330 ± 200	28,610 B.C. (95.4%) 27,620 B.C.
Site 10	LTL12218A	North of Duguna	7°3'9.10"N	37°58'24.00"E	Debris[b]	12,411 ± 100	13,070 B.C. (95.4%) 12,100 B.C.
Site 10	LTL12219A	North of Duguna	7°3'9.10"N	37°58'24.00"E	Debris[b]	13,902 ± 100	15,430 B.C. (1.1%) 15,380 B.C. 15,290 B.C. (94.3%) 14,790 B.C.
Site 17	LTL12220A	Bedessa	6°52'40.40"N	37°56'43.80"E	Debris[b]	17,486 ± 90	19,330 B.C. (95.4%) 18,470 B.C.
Site 18	LTL12221A	Northeast of Bedessa	6°54'27.00"N	37°58'24.50"E	Debris[b]	10,887 ± 70	11,000 B.C. (95.4%) 10,650 B.C.

[a]Radiocarbon dating by high-resolution accelerator mass spectrometry (AMS) has been performed at the Centro di Datazione e Diagnostica (CEDAD), Dipartimento di Ingegneria dell'Innovazione, Università del Salento, Brindisi (http://cedad.unisalento.it/). See *D'Elia et al*. [2004] for details of sample preparation for the AMS measurements. Latitude and longitude of sample locations assume WGS84 datum.
[b]Organic matter contained in the faulted debris.

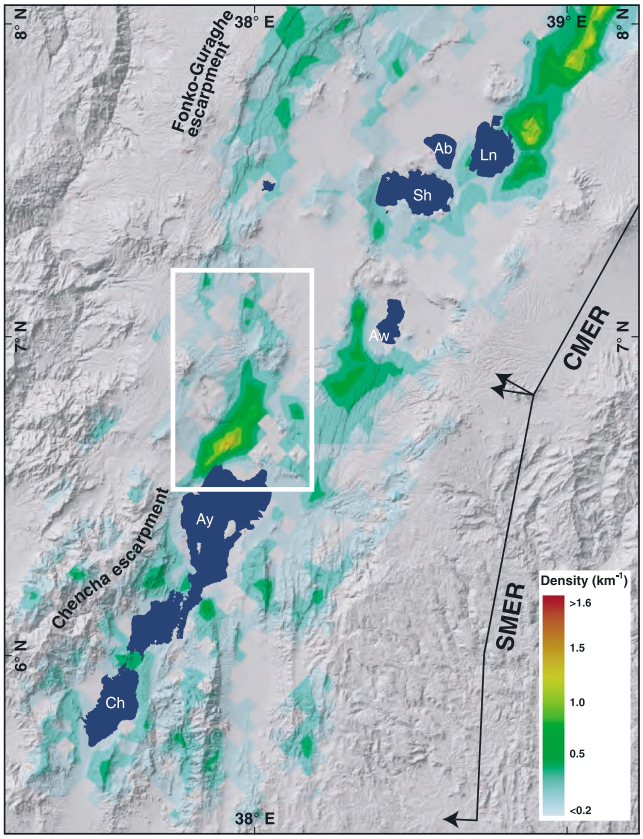

Figure 4. Map of fault density in the Southern and Central MER (SMER and CMER, respectively) superimposed onto a shaded relief of the study area [after *Agostini et al*., 2011a]. Fault density has been calculated by using the fault data set reported in Figure 1. The density has been calculated for 5 km sided square cells as the ratio between the cumulative length of faults contained in each cell and the area of the cell, over a grid that is oriented nearly parallel to the overall envelope of the fault network (approximately NE-SW). The white box indicates the study area illustrated in Figures 2 and 3.

boundary faults [e.g., *Hayward and Ebinger*, 1996]. Although affected by an Early Miocene deformation phase related to the northern propagation of the Kenya Rift, significant slip on boundary faults occurred during the Pliocene [*Bonini et al*., 2005]. No radiometric dating of faulted material is currently available for this area, although analysis of historical seismicity [*Gouin*, 1979; *Keir et al*., 2006] suggests these faults to accommodate the largest part of recent and active deformation; the axial deformation is practically negligible in the Southern MER [*Hayward and Ebinger*, 1996; *Agostini et al*., 2011a]. Significant marginal deformation in the Southern MER is also supported by morphotectonic analysis in the Arba Minch-Bridge of God area (Figure 1) [*Boccaletti et al*., 1998], as well as by recent GPS data indicating localized active deformation along the Chencha escarpment in the western rift margin [*Kogan et al*., 2012]. Similarly to the Central MER, areas of Quaternary volcanic activity in the Southern MER are limited to the rift margins (e.g., Soddo area, see below), except for the limited basaltic activity that gave rise to the land bridge (Bridge of God) separating Lake Abaya from Lake Chamo (Figure 1) [e.g., *Zanettin et al*., 1978; *Ebinger et al*., 1993; *George and Rogers*, 1999; *Rooney*, 2010; *Rooney et al*., 2011]. However, differently from the Central MER, the geometry of the two tectono-magmatic belts of the WFB and Silti-Butajira-Debre Zeyt is less clear in the Southern MER; these two belts are believed to interact and possibly overlap between latitudes 6.5°N and 7°N [e.g., *Rooney*, 2010; *Rooney et al*., 2011]. No detailed geophysical studies are available for the Southern MER, and the subsurface rift architecture remains poorly constrained in this MER sector. The few geophysical data indicate, consistent with a limited volcanic activity within the rift depression, the absence of significant magmatic processes in this area [*Dugda et al*., 2005]. Overall, the above observations point to a further decrease in extension and magmatic modification passing from the Central to the Southern MER. Notably, the transition between these two rift sectors occurs (at around latitude 7°N) in correspondence to a major E-W-trending transverse structure (Goba-Bonga lineament of *Abbate and Sagri* [1980]), likely related to the reactivation of a preexisting lithospheric weakness zone [e.g., *Bonini et al*., 2005] and expressed in the Ethiopian Plateau by normal faults and grabens [e.g., *Boccaletti et al*., 1998].

[6] The evolution of the different MER sectors has been controlled by the extension between the major Nubia and Somalia Plates, which is now occurring in a roughly N100° E direction at rates of 4–6 mm/yr as constrained by geodetic, seismic, geological and plate motion data [e.g., *Corti*, 2009, and references therein; *Agostini et al*., 2011a; *Kogan et al*., 2012]. Due to the localization of extensional deformation along a N- to NE-SW-trending lithospheric-scale preexisting heterogeneity [e.g., *Keranen and Klemperer*, 2008], this extension direction gave rise to conditions of oblique rifting in the MER, with a decrease in rift obliquity proceeding from the Northern MER southward [*Agostini et al*., 2011a].

3. Geology of the Soddo Area

[7] The Soddo area is located on the western margin of the Southern MER, close to the transition zone with the Central MER, between the major escarpments of Chencha and Fonko-Guraghe. It extends from the northern coast of Lake Abaya, to the south, up to the town of Durame, to the north (Figures 1 and 2). As typically occurring in the MER, most of the rift floor and margins in the Soddo area are covered by volcanic and volcano-sedimentary rocks associated with the main rifting events (Figure 2). The most important geologic units are outlined below from the oldest to the youngest.

[8] The lowermost unit corresponds to the Tertiary basaltic sequences (Nb in Figure 2) that cover large areas of Ethiopia and are comprehensively known as Plateau Flood basalts or Trap Series [*Mohr and Zanettin*, 1988, and references therein]. These basalts represent the first volcanic activity related to the Tertiary rifting in Ethiopia, although this volcanic phase predates the main rifting events [e.g., *Abebe et al*., 2005; *Bonini et al*., 2005]. In the Soddo-Arba Minch area, the mildly alkaline basaltic lava flows are about 30–36 Ma in age [*Zanettin et al*., 1978], and crop out at the northern termination of the Chencha escarpment.

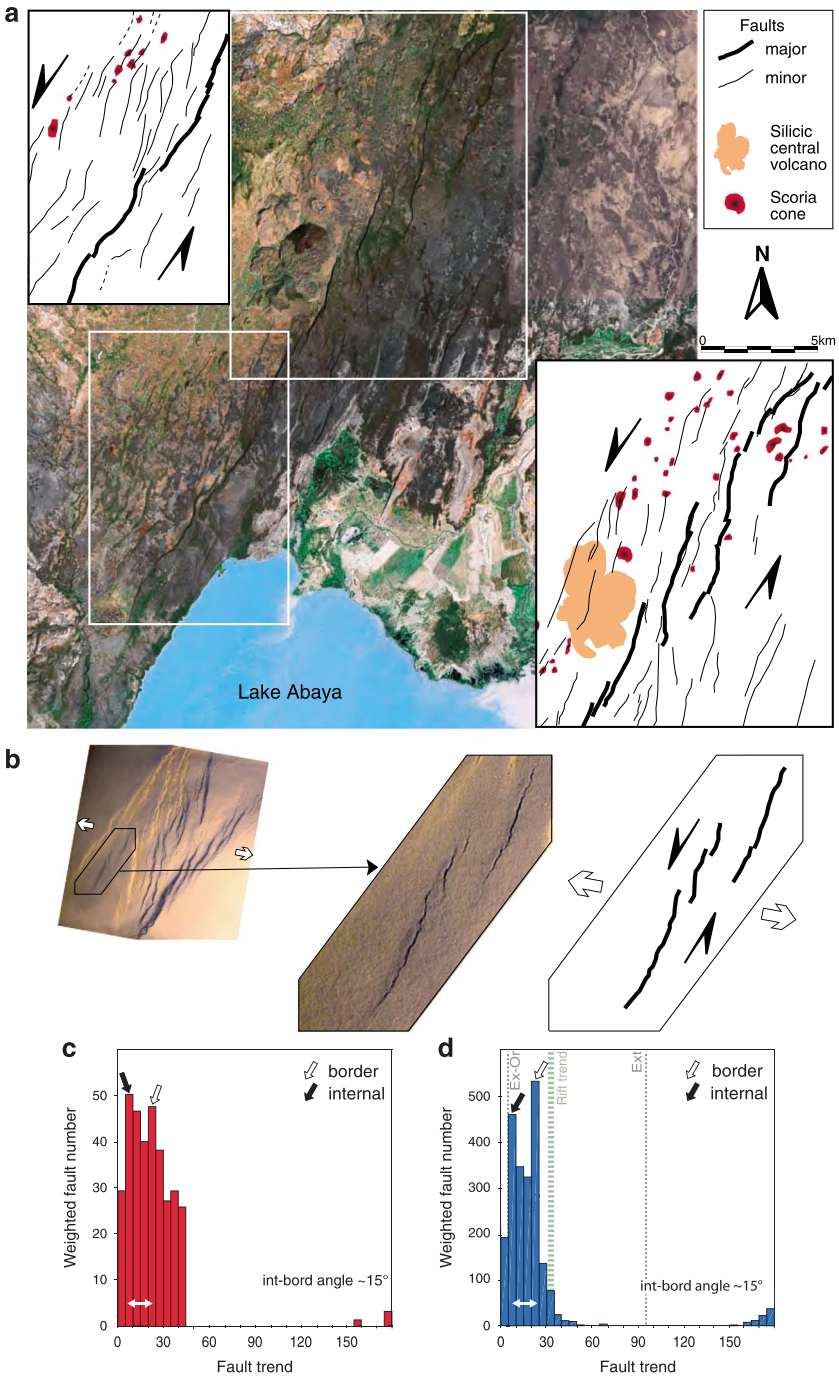

Figure 5. (a) Landsat image and structural interpretations of the fault system between Lake Abaya and the Hobitcha caldera. Note the sigmoidal, right-stepping *en-echelon* faults that likely reflect a sinistral component of motion along the western rift margin [*Boccaletti et al.*, 1998]. (b) Detail of small-scale, analog model of low-obliquity rifting [*Corti*, 2008] with structural scheme showing the *en-echelon* fault pattern resulting from the left-lateral transcurrent component of motion (modified from *Corti* [2009]). (c) Weighted fault distribution in the Soddo area, illustrated as histogram of the fault trends. The weighting factor for each fault is the ratio between the fault length and the minimum length of the whole data set, such that long faults have higher ratio (weight) than short ones. The frequency of the azimuth of a fault directly relates to this ratio: the longer the fault, the higher its frequency. Note the two peaks at N5–10°E and N20–25°E corresponding to the boundary and internal faults, respectively. Int-bord angle is the angle between internal and border faults. (d) Weighted fault distribution in a low-obliquity rifting model ($\alpha = 30°$, where α is the angle between the rift trend and the orthogonal to the direction of extension), illustrated as histogram of the fault trends [after *Agostini et al.*, 2011a]. Ex-Or: orthogonal to the extension direction; Ext: extension direction. Note the similarity between the model and natural structural pattern.

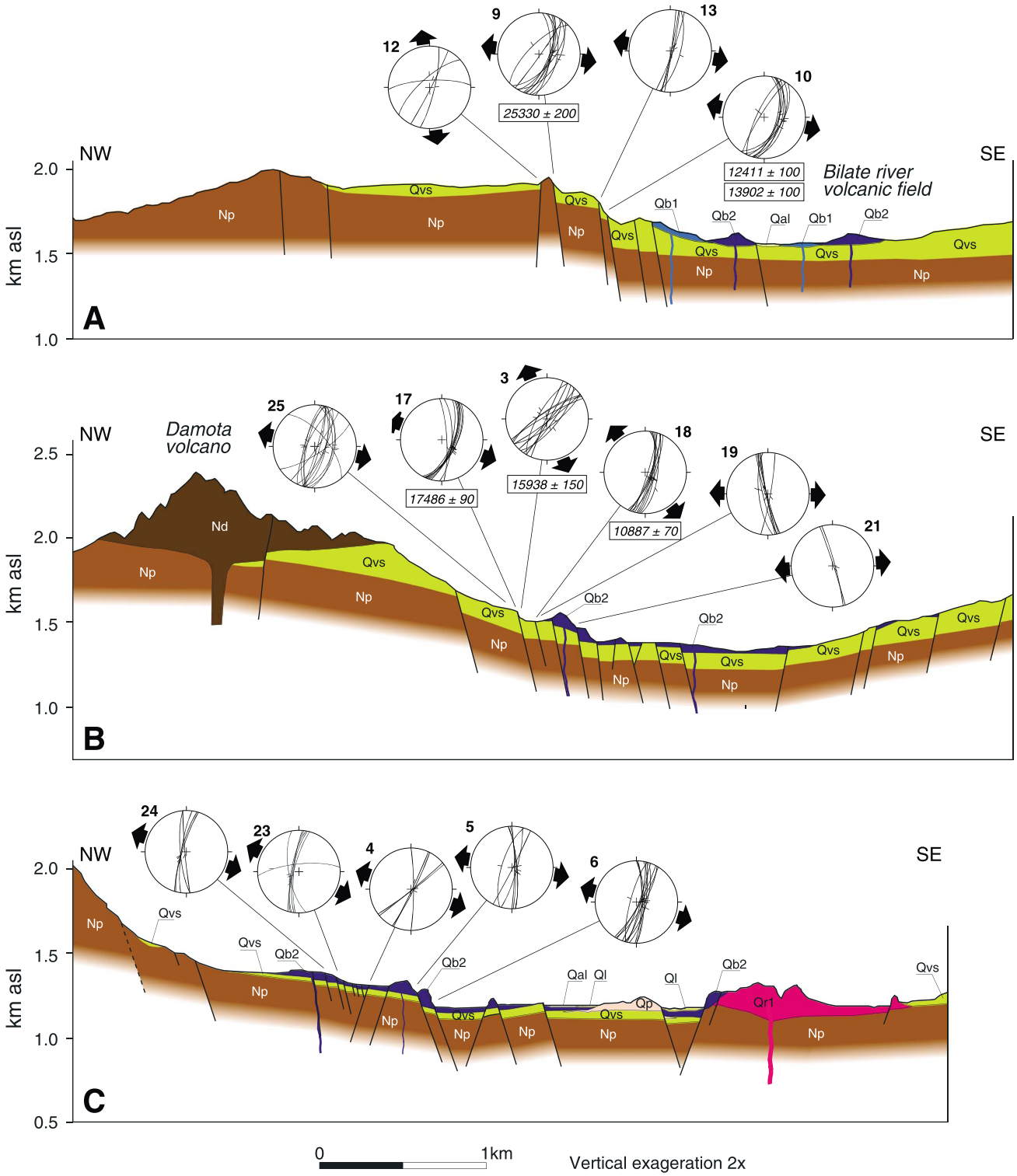

Figure 6. Geological cross sections through the study area (locations in Figures 2 and 3). Stereographic projections (Wulff net, lower hemisphere) display the fault planes and the collected associated fault slip vectors; black arrows indicate the obtained direction of extension (see text and Table 1; location in Figure 3). The new radiometric dating of faulted material is also reported. Symbols as in Figure 2.

[9] Although Miocene volcanic activity has been reported in regions north and south of Soddo [e.g., *Bonini et al.*, 2005; *Rooney*, 2010], no time-correlative volcanism is present in the study area. The flood basalt flows are overlain by Pliocene peralkaline pantelleritic ignimbrites (Nazret pyroclastics, Np in Figure 2) that characterize large portions of the western plateau northwest of Lake Abaya. These ignimbrites are time-correlative with the Nazret pyroclastic

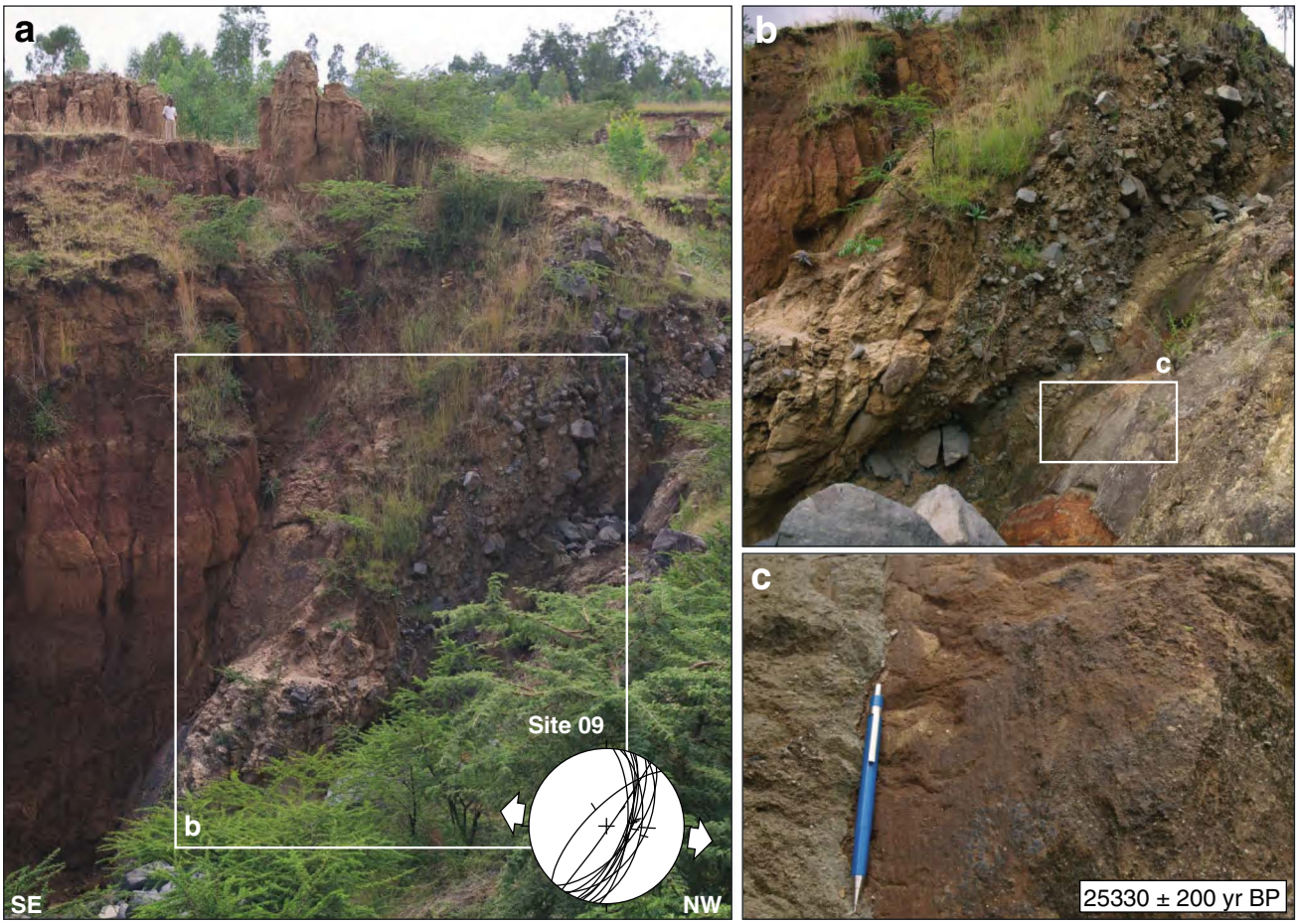

Figure 7. Characteristics of the major normal fault at site 9. (a) Panoramic view of the fault zone; (b) detail of the thick fault breccia; (c) close-up of the fault plane showing well-developed striations to the right of the pen (numbers refer to the radiocarbon dating; see Table 2). The paleostress analysis of the fault slip data collected on the fault plane (illustrated in the right-bottom corner of Figure 7a) indicates a N98°E-directed extension.

rocks of the Northern and Central MER [*Abebe et al*., 2005], and with the Chewkare Ignimbrites of *Chernet* [2011]; the voluminous eruption of acidic pyroclastic deposits of the Nazret Unit is believed to mark the onset of rifting in the MER [*Bonini et al*., 2005]. Ages of ~4 Ma are reported for these ignimbrites in the area [see *Chernet*, 2011].

[10] A large silicic volcanic complex (Damota volcano), which rises over 1000 m from the surrounding rift escarpment, locally overlies the Nazret pyroclastic rocks (Figure 2). The trachytic lava flows from Damota (Nd in Figure 2) are of Late Pliocene age (~2.9 Ma [*Woldegabriel et al*., 1990]), although some morphological characteristics suggest that activity might have continued into the Quaternary [*Chernet*, 2011]. Worth noting, the Pliocene activity at Damota has been related to a phase of rift-margin volcanism associated with the transverse, roughly E-W Goba-Bonga structure [*Abbate and Sagri*, 1980], also responsible for the E-W alignment of eruptive centers in the Wagebeta volcanic complex close to Durame (Figure 2) [*Woldegabriel et al*., 1990].

[11] The Pliocene units are covered by complex Pleistocene sequences made of alluvial and rare lacustrine sediments with interbedded pyroclastics and rare basalt flows (Qvs in Figure 2). A wide area north of Lake Abaya is covered by horizontally bedded yellowish brown poorly hardened siltstone, mudstone with interbedded reworked and waterlain pumice. Quaternary volcanic centers (such as Hobitcha) have supplied large quantities of pyroclastic material to this ancestral lacustrine system, together with basaltic flows evident as hyloclastite layers in some sections of this unit [*Chernet*, 2011]. A single dating of a trachytic rhyolite near Boditi gave an age of ~1.6 Ma [*Zanettin et al*., 1978], whereas correlation of these alluvial deposits with similar sediments north of the study area is consistent with a sedimentary sequence spanning the end of the Middle Pleistocene to the Upper Pleistocene-Holocene, as also supported by analysis of the archeological remains embedded within these sediments [*de la Torre et al*., 2007].

[12] Quaternary rhyolitic volcanic centers have produced large volumes of peralkaline lava flows and domes (Qr1, Qr2, and Qr3) and pyroclastic deposits (Qp) with earlier members intercalated with lacustrine sediments. The earliest phase of rhyolitic volcanism in the Quaternary was associated with the Hobitcha rhyolitic center, a horseshoe-shaped caldera with a diameter of ~10 km that exposes large volumes of lava and pyroclastic products on its flanks and caldera rim.

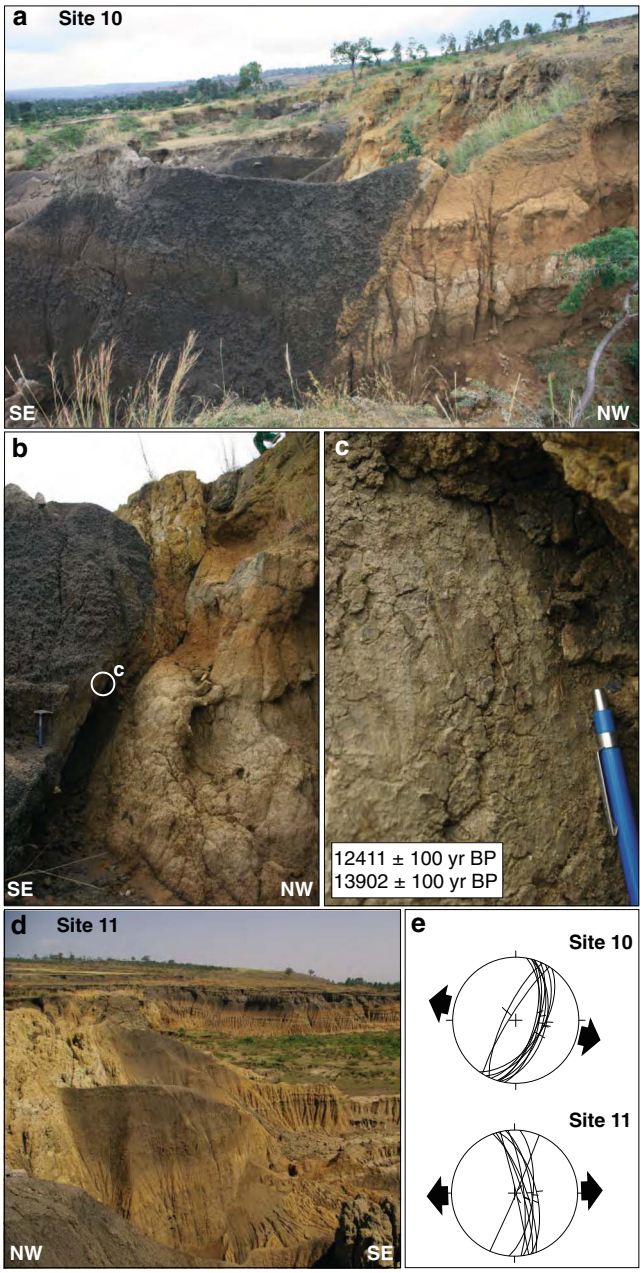

Figure 8. (a) Panoramic view of the normal fault at site 10; (b) detail of the fault zone; (c) close-up of the fault plane showing well-developed striations to the left of the pen. Numbers refer to the radiocarbon datings (see Table 2). (d) Panoramic view of the normal fault at site 11. (e) Paleostress analysis of the fault slip data collected at sites 10 and 11, indicating a direction of extension of N103°E and N88°E, respectively.

A K-Ar age of 1.57 Ma has been reported for a rhyolite flow (Qr1) from the inner caldera wall of this rhyolitic center [see *Chernet*, 2011]. Duguna volcano is the most prominent of the Quaternary volcanic centers, with a base diameter of about 10 km and a summit caldera, which produced pumice and ashfall deposits (Qp) with a thickness of >30 m (Figure 2). A large caldera collapse likely characterized this volcanic complex, with the outline of the collapse structure marked by smaller rhyolite domes to the southeast. Ages of 430–460 ka have been reported for the eastern flank of the Duguna volcano [*Bigazzi et al.*, 1993]. Other rhyolitic volcanic centers (such as Chericha, Figure 2) are found along the axis of the rift, although very recent obsidian and pitchstone flows (Qr3)—probably representing the youngest rhyolitic activity in the study area—are located along the rift margin, at the southern edge of the Hobitcha caldera (Salewa Dore and Hako rhyolitic centers, Figure 2). These latter centers are also characterized by ongoing fumarolic activity [*Chernet*, 2011].

[13] The Quaternary-recent volcanic activity is also characterized by widespread basaltic volcanism (Qb1 and Qb2 in Figure 2), which mostly occupies a broad area between Lake Abaya and Duguna. As in other MER sectors, basaltic lava flows, scoria, and phreatomagmatic deposits (typically referred to as Wonji basalts; see, for instance, *Abebe et al.*, [2005]) are associated with the recent fault systems affecting the rift valley, with evident alignments of scoria cones marking the main fault swarms [e.g., *Rooney et al.*, 2011; *Mazzarini et al.*, 2013]. Together with the above-described Quaternary acidic rocks, this basaltic activity gives rise to the typical bimodal volcanism that characterizes this continental rift [e.g., *WoldeGabriel et al.*, 1990]. The oldest basalts of this unit are in places interstratified with the earlier succession of the lacustrine sediments (Qvs). The youngest episodes of basaltic eruptions seem to be associated with the intense faulting that characterizes the rift margin in correspondence to the Hobitcha caldera. Fumarolic activity is reported for basaltic centers south of the Duguna volcano (Figure 2).

[14] The most recent deposits in the area correspond to Holocene lacustrine sediments (Ql) related to the recent fluctuations of Lake Abaya, and to fluvial sediments (Qal) deposited by two major rivers (Bilate and Gidabo), which drain most of the study area and have formed lacustrine deltas a few kilometers wide on the northern part of the lake.

4. Analysis of Quaternary Volcano-Tectonic Activity in the Soddo Area

[15] During different field surveys between 2007 and 2013, extensive fieldwork in the study area (Figures 2 and 3) was conducted in order to characterize the architecture and kinematics of the main fault systems, as well as their timing of activity. Fieldwork was preceded by interpretation of satellite images (Landsat TM, Aster, and other available images, e.g., Google Earth imagery) and digital elevation models (Aster, 30 m resolution; Shuttle Radar Topography Mission, SRTM, 90 m resolution). The aims of this remote sensing study were as follows: (1) detailed mapping of fault traces, (2) morphotectonic analysis of the main structures (including an analysis of the local hydrographic pattern, see below), (3) first-order definition of the relations between structures and volcanic centers, and (4) selection of key areas for the fieldwork. The latter consisted of (1) analysis of the morpho-tectonic structures recognized through the remote sensing study, (2) structural analysis of the fault planes, (3) identification and sampling of recent rocks affected by faults, and (4) a more detailed investigation of the relations between faulting and volcanism. Kinematic indicators on fault planes and strikes and dip of faults were measured in order to calculate paleostress axes orientations through the right dihedron

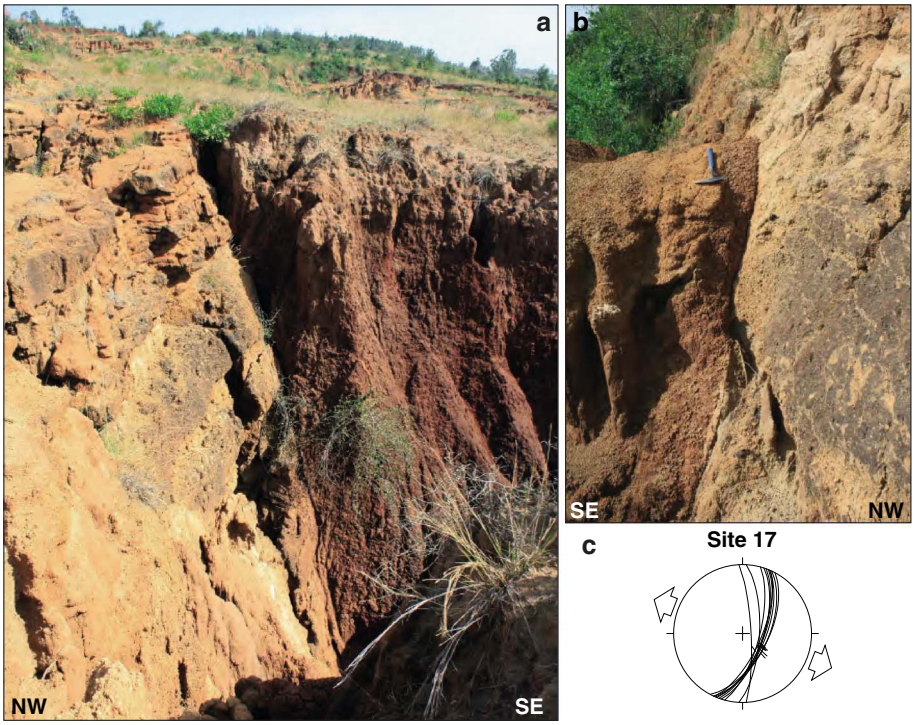

Figure 9. (a) Panoramic view of the normal fault at site 17; (b) detail of the fault zone; (c) paleostress analysis of the fault slip data collected on the fault plane, indicating a N110°E-directed extension.

inversion method [*Angelier and Mecheler*, 1977; *Angelier*, 1979]. The database consists of 25 sites of measurements (location in Figure 3), and the results of calculations are listed in Table 1 and illustrated in the following sections. The age of faulted rocks has been established on the basis of available geological maps. New C14 radiometric age determinations of very recent rocks involved in faulting (in general composed of fine breccias or sediments smeared on the fault plane) have also been performed (Table 2). The distribution and characteristics of faulting are illustrated below through description of the plan view fault pattern, geological cross sections across the margin (used to illustrate the characteristics of faulting, the age of deformation, and the paleostress data), and the relations between faults and the recent volcanic activity in the area.

4.1. Plan-View Fault Pattern

[16] Pervasive deformation affects the western rift margin southeast of Soddo, giving rise to a complex system of roughly N20°E to N25°E-trending border faults; more limited faulting affects the rift floor northeast of Lake Abaya, with a set of N5°E to N10°E-trending internal (Wonji) faults (Figure 3). The border fault system is characterized by numerous closely spaced faults, resulting in the highest fault density of the whole Southern MER (Figure 4). This fault system is made of a typical array of sigmoidal, right-stepping *en-echelon* normal or oblique faults, with limited lateral extent (maximum length in the range of a few kilometers) and limited vertical offset (typically in the range of a few tens of meters, and up to 150–200 m). These faults are particularly evident north of Lake Abaya (Figure 5a), where they control the development of small Quaternary basins and the location of recent volcanic centers (see below). This sigmoidal, *en-echelon* arrangement of faults likely reflects a sinistral component of motion along the western rift margin [*Boccaletti et al.*, 1998]. In fact, these faults have been suggested to have formed in relation to an oblique reactivation the roughly NE-trending northern segment of the Chencha escarpment under a roughly E-W extension [*Boccaletti et al.*, 1998]. Comparison of the fault pattern with the deformation resulting from analog models of oblique rifting (Figure 5b) [*Corti*, 2008] supports this observation. In particular, detailed comparison of the fault orientation distribution suggests that the fault pattern in the Soddo margin is compatible with a sub-E-W (N95°E to N100°E) extension direction (Figure 5c), resulting in an oblique extension with respect to the roughly NE-SW-trending rift. Under these conditions, the border faults follow as a group the trend of the rift margin but are individually oriented obliquely to both this trend and the orthogonal to the extension direction (Figure 5c); they form orthogonal to a local direction of extension that corresponds to the bisector of the angle between the plate motion vector and the normal to the rift trend (Figure 5c) [e.g., *Corti et al.*, 2013]. Instead, axial faults form perpendicular to the regional extension direction (Figure 5c).

4.2. Characteristics of Deformation, Age of Faulting, and Paleostress Analysis

[17] Three NW-SE-trending geological cross sections transecting the western margin are used to illustrate the characteristics of deformation in the Soddo area, as well as the age of faulting and the paleostress information resulting from inversion of the collected fault slip data. From north to south, the cross sections span the Durame-Duguna-Bilate river

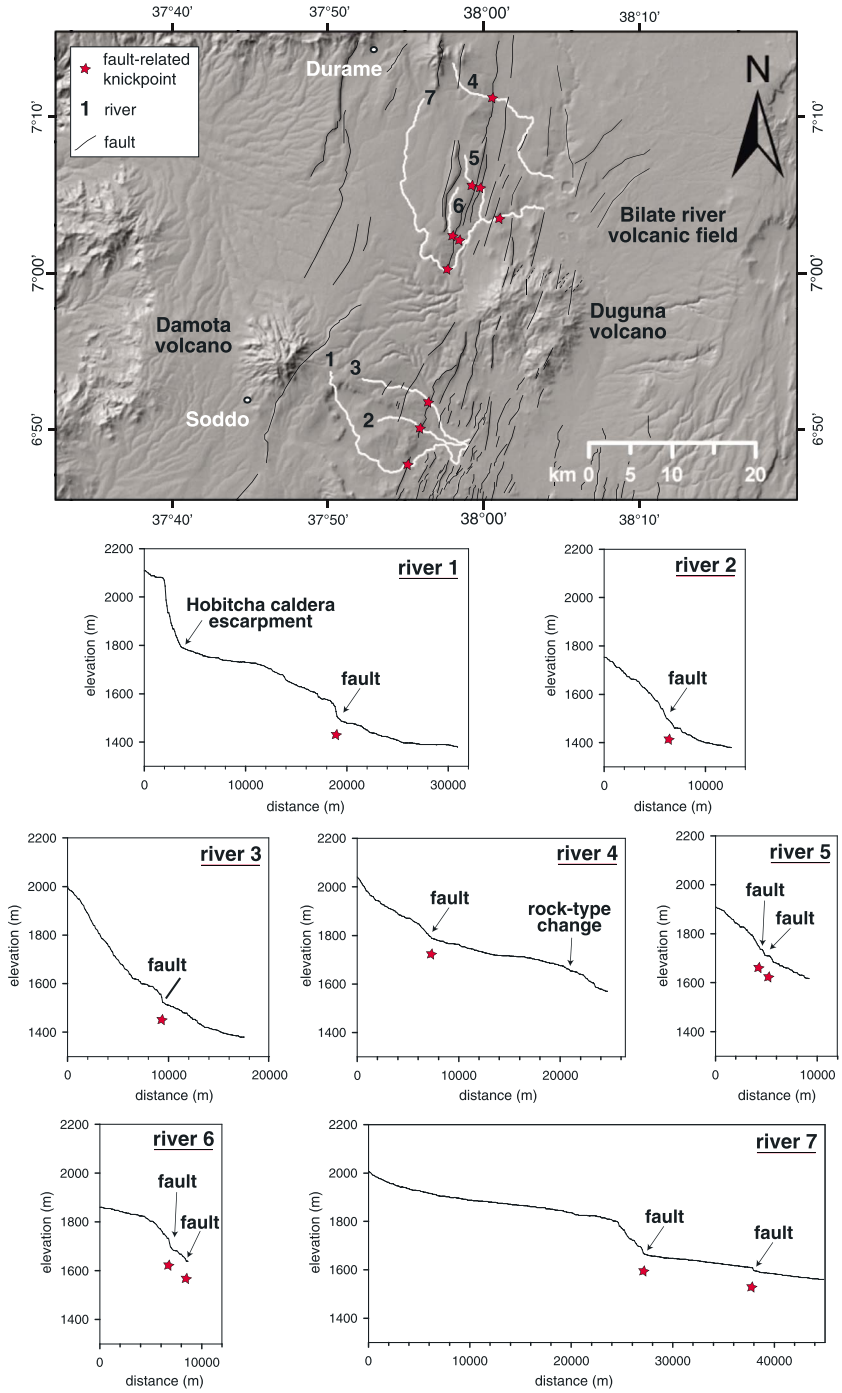

Figure 10. (a) Map of the study streams draining the rift margin east of Soddo and Durame. Red stars indicate the location of fault-related knickpoints. (b) Stream longitudinal profiles, extracted from SRTM DEM sampling topography every 100 m.

volcanic field, Damota-Soddo, and North Lake Abaya areas (Figure 6).

[18] The northernmost cross section clearly illustrates a localization of normal faulting at the rift margin typical of this area (cross section A in Figure 6). Here the transition from the plateau to the rift floor occurs through a few normal faults that affect both the Nazret pyroclastics (Np; Figures 2 and 6) and the overlying Pleistocene volcano-sedimentary successions (Qvs; Figures 2 and 6). These faults are mostly SE-dipping, even if some NW-dipping structure are observed, and are characterized by maximum vertical throw on the order of ~100 m. Typically, the faults have well-developed fault zones, which normally allow very good structural analysis. This is exemplified by site 9, where a 5–6 m thick fault breccia occurs along the fault (Figures 7a and 7b); organic matter contained in rocks smeared along minor fault planes allowed C14 dating, which gave an age of 25,330 ± 200 years B.P. for this fault (Figure 7c; Table 2).

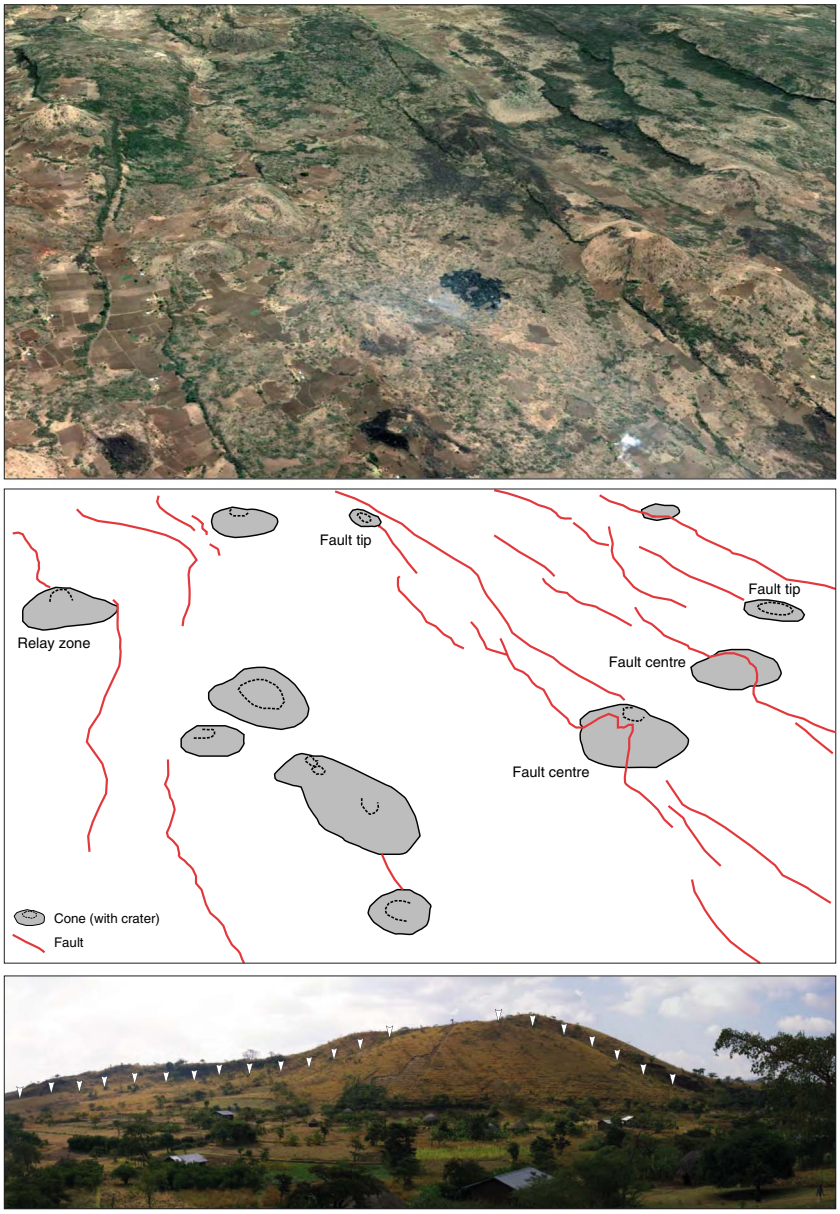

Figure 11. (top) Three-dimensional view of satellite imagery (Google Earth image) and (middle) structural interpretation illustrating the typical location of basaltic spatter cones with respect to major normal faults (the area is located ~6 km NNE of the Salewa Dore center). (bottom) Photo showing a basaltic spatter cone cut by a normal fault (base of the fault scarp indicated by the white arrows).

Assuming this dating as a minimum age for the fault, and considering a cumulative scarp of ~100 m, the rough estimate of the maximum vertical slip rate is ~4 mm/yr for this structure. The occurrence of ignimbrites along the fault plane favored the formation of kinematic indicators, whose inversion resulted in a roughly ESE-WNW direction of extension (Figure 7a). Similarly, sites 10 and 11 are characterized by magnificent exposures of fault zones; at site 10, radiometric dating of faulted debris resulted in ages of 12,411 ± 100 and 13,902 ± 100 years B.P. (Figure 8; Table 2), resulting in a rough estimate of the maximum vertical slip rate of ~5 mm/yr, considering a cumulative scarp of ~60 m. Again, inversion of kinematic indicators on the fault resulted in a roughly E-W to ESE-WNW direction of extension (Figure 8). Overall, analysis of fault slip data collected on faults along this transect shows a strong coherence of data (sites 8, 9, 10, 11, and 13) in terms of stress orientation, with the only exception of site 12 located at the northern termination of a small horst (Figures 3 and 6; supporting information).

[19] The central transect (cross section B in Figure 6) is located in correspondence to the volcanic centers of Damota and Hobitcha. In this case, the rift margin is marked by the occurrence of many faults with limited vertical displacements in the order of a few tens of meters, giving rise to a smoother topography with respect to what was observed in the northernmost transect. The faults are always very steep and dip to the SE, whereas in the more axial portions of the rift, they show a consistent northwestern dip (Figure 6).

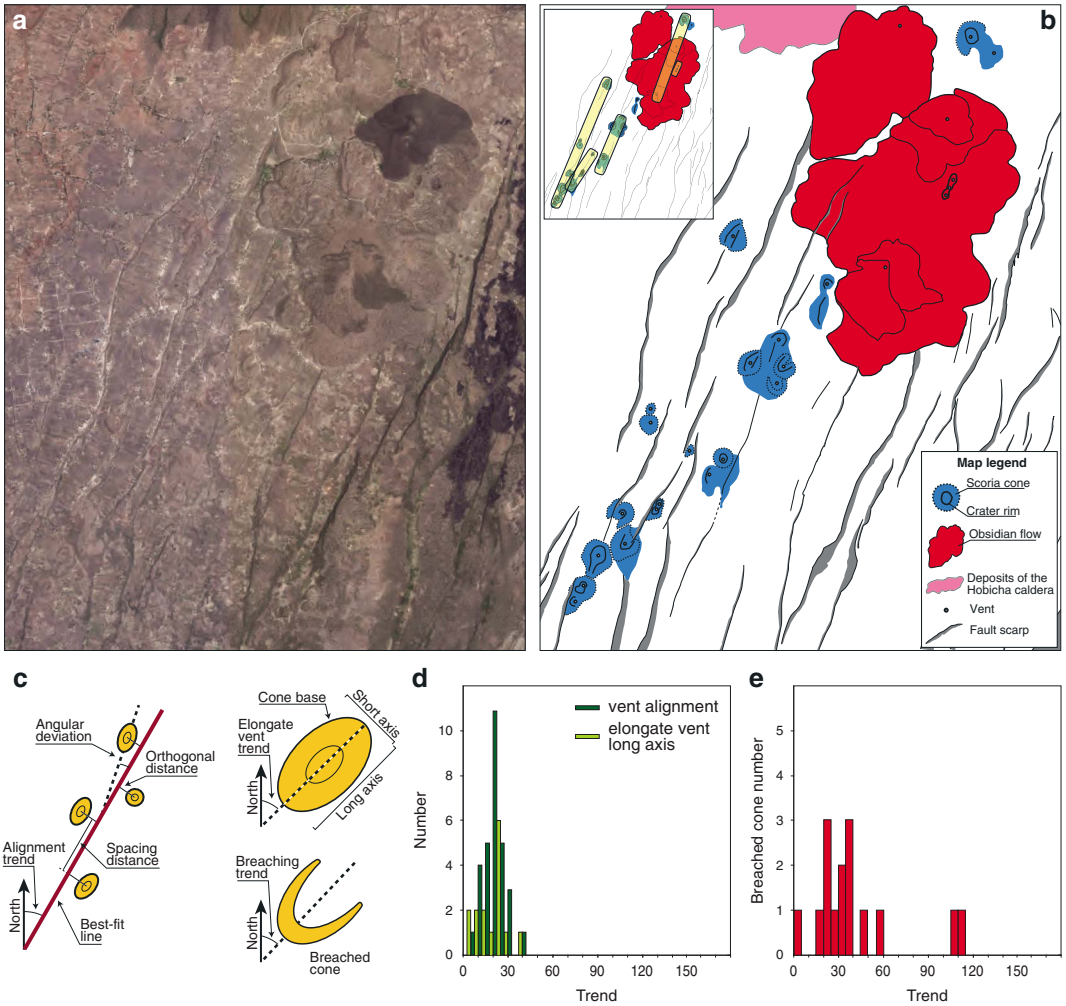

Figure 12. Relations between eruption vents and faulting illustrated as (a) satellite image and (b) structural interpretation of the area close to the Salewa Dore and Hako centers. Inset shows the main vent alignments (brownish shading), defined on the basis of both the visual analysis of the spatial distribution of vents and the analysis of their elongation. (c) Schematic representation of attributes used to characterize and assess vent shape and vent alignments [after *Paulsen and Wilson*, 2010]. The best fit line for an alignment is calculated by minimizing the orthogonal distances from points to the line. The angular deviation of elongate vents from the best fit line is measured as the acute angle separating the long axis of the elongate vent and the best fit line. Vent spacing distance is defined as the distance that separates adjacent vents found along the trace of the best fit line. The axial ratio for single cones is calculated as the ratio between the lengths of the long and short axes of the best fit ellipse matching the mapped shape of the vent (vents are considered elongate when the axial ratio is >1.2 [*Paulsen and Wilson*, 2010]). (d) Azimuthal distribution of vent alignment and elongate vent long axis; (e) azimuthal distribution of cone breaching (calculated by considering the long axis of the breached area).

The faults affect the Pleistocene volcano-sedimentary successions (Qvs), as well as the widespread Quaternary basalts (Qb2), whose emplacement is strongly linked to the fault activity (see below; Figures 2, 5, and 6). Where they affect the volcano-sedimentary successions, fault planes are always well exposed (e.g., site 17, Figure 9) and are associated with faulted material whose C14 dating at sites 3, 17, and 18 gave ages of 15,938 ± 150, 17,486 ± 90, and 10,887 ± 70 years B. P., respectively (Figures 3 and 6; supporting information; Table 2). In this case, the rough estimates of the maximum vertical slip rate are of ~3 mm/yr for site 3 (cumulative scarp of ~50 m), ~1 mm/yr for site 17 (cumulative scarp of ~20 m), and ~9 mm/yr for site 18 (cumulative scarp of ~100 m). The structural analysis of faults results in a direction of extension ranging from NW-SE to E-W, mainly depending on local fault orientation (Figure 6; supporting information; Table 1); worthy of note, the E-W orientation of extension direction mainly occurs along the rift axis (Figure 3, sites 7, 19, 20, and 21).

[20] The southernmost cross section (C in Figure 6) crosses the rift valley north of Lake Abaya (Figure 3). As in the central transect, the transition between the rift shoulder and the floor occurs through the occurrence of many minor faults with minor vertical throw dipping toward both the SE and the NW. The faults affect the Quaternary (Qb2) basalts that largely crop out in the southern part of the study area. A

Table 3. Geometrical Parameters for the Volcanic Vents Analyzed in the Soddo Area[a]

Alignment Number	Lat, Long (Baricenter)	Rock Type[b]	Length (m)	Number of Vents	Number Elongate Vents[c]	Standard Deviation Best Fit Line Orthogonal Distance (m)	Standard Angular Deviation Vent Long Axes (°)	Average Vent Spacing Distance (m)	Alignment Azimuth (°)	Average Vent Long Axis Azimuth (°)	Reliability Grade[d]
1	6°40'01", 37°51'44"	B	2800	5	2	41	9.2	588	22	27	A
2	6°40'02", 37°52'04"	B	1600	3	2	53	2	810	36	33	B
3	6°40'42", 37°52'47"	B	2300	5	3	110	2.3	705	24	27	A
4	6°42'43", 37°54'13"	R	3500	4	1[e]	35	–	1300	19	–	A
5	6°42'23", 37°54'19"	R	400	3	3	6	1.5	120	22	24	B
6	6°44'42", 37°50'54"	B	4300	4	1	71	13	1400	9	22	D
7	6°45'23", 37°54'58"	B	2500	6	1	85	5.5	520	12	23.5	A
8	6°45'39", 37°55'30"	B	3200	6	0	170	–	670	4	–	D
9	6°46'33", 37°57'12"	B	5300	4	0	60	–	1760	22	–	D
10	6°47'14", 37°56'40"	B	5400	12	3	80	8.5	340	24	16	A
11	6°45'41", 37°58'55"	B	3150	5	0	110	–	800	26	–	C
12	6°45'23", 38°04'23"	B	5600	14	1	240	7	1020	14	21	D
13	6°50'16", 37°59'33"	B	2200	6	1	110	7	560	23	30	C
14	7°02'43", 38°03'17"	B	4300	3	0	220	–	1500	8	–	D
15	7°02'33", 38°05'20"	B	8600	4	0	300	–	2970	4	–	D

[a]Adapted from *Paulsen and Wilson* [2010]. Latitude and longitude of alignment locations assume WGS84 datum.
[b]B, basalts; R, rhyolites.
[c]A vent is considered elongated when the ratio between the lengths of the maximum and minimum axes of the best fit ellipse matching the mapped shape of the vent is >1.2.
[d]Fissure ridge.
[e]Reliability grade: A > B > C > D.

limited number of normal faults, giving rise to local small grabens, characterize the axial portion of the rift north of Lake Abaya. Differently from faults affecting the Pleistocene volcano-sedimentary successions, the normal faults cutting the Quaternary basalt flows are not characterized by the presence of fine fault breccias and/or faulted debris along the fault plane, so that no samples for C14 dating have been collected along this transect. In addition, these structures do not typically display good exposition of fault planes, so that analysis of kinematic indicators on these structures is normally of a lower quality. In fact, faults in the basalts rapidly degrade, splitting along individual columnar basalts and leading to near-vertical scarps that rarely preserve the fault slip plane [*Casey et al*., 2006]. However, although with local variation (e.g., site 1 and 16) mainly due to local perturbations (e.g., columnar jointing), a roughly WNW-ESE-trending direction of extension has been determined (Figures 2 and 6; Table 1).

[21] The above results indicate significant extensional deformation at the western rift margin, mostly characterized by sets of numerous, small-offset normal faults; dating of organic matter involved in faulting gave minimal ages of fault activity spanning from the latest Pleistocene to the Holocene (Table 2). The inversion of fault slip data, although with local variations, shows a well-defined direction of extension oriented WNW-ESE to E-W (see cumulative plot of data in Figure 3).

4.3. Analysis of Local Hydrography and Relations With Recent Fault Activity

[22] Geological data were integrated through a geomorphic analysis aimed at the investigation of the local hydrographic pattern and its possible relations to recent tectonic activity (Figure 10). In the Soddo area, channels both parallel and perpendicular to tectonic structures characterize hydrography. The narrow river valleys present mostly subvertical slopes indicating the dominance of incision on lateral erosion. Important variations in the fluvial network pattern are observed in correspondence to major and minor faults: in particular, channels are characterized by abrupt changes in direction when they cross fault planes; also, when the main channels cut across fault planes, their valleys change in width in response to a variation in local base level that alternatively can induce an increase in incision or lateral erosion. Minor channels often disappear passing from the hanging wall to the footwall as if they are beheaded; this suggests that hydrography is not yet developed in correspondence to fault scarps. Moreover, when the streams cut through faults, strong variations in channel gradient occur, generating knickpoints, which are apparent in the field as well as in the river longitudinal profiles (Figure 10). Generally speaking, river long profiles are concave up, a shape traditionally equated to a river in equilibrium [*Mackin*, 1948]. This form depends partially from the fact that since discharge increases and grain size decreases downstream, lower gradients are progressively needed to transport channel alluvium [*Leopold et al*., 1964] as well as to incise bedrock [*Pazzaglia et al*., 1998]. Deviations from the smooth, concave up shape indicate that the river is in a transient state of disequilibrium in response to a base level, tectonic, climatic, or rock-type perturbation. These deviations are convex segments called knickpoints or knickzone according to their length. The longitudinal profiles of study rivers are just slightly concave, but often they are straight or even convex (Figure 10). They are also characterized by knickpoints and knickzones that correspond to faults in the structural-geological maps (Figures 2, 3, and 10).

[23] In summary, the hydrography of the study area appears to be strongly influenced by tectonics, in terms of both structure location as well as variations in tectonic rates. Indeed, valley and channel features indicate that the rivers are incising the high erodible Qvs in response to recent tectonic inputs. In correspondence to fault scarps, hydrography is not yet developed, likely as a consequence of recent scarp growth. The changes in valley width when channels cut across faults indicate varied river adjustment to variations in local base level related to different tectonic rates. This state of disequilibrium is confirmed by the shape of river longitudinal profiles (Figure 10) that is strongly disturbed by fault-related knickpoints and characterized by low concavity.

[24] These observations are in agreement with a very recent activity of normal faults on the western rift margin at Soddo.

4.4. Relations Between Faulting and Volcanic Activity

[25] There is a close correlation between the recent volcanic activity and faulting in the Soddo area. Figure 2 clearly displays a close association between outcrop of the widespread Quaternary basalts and the numerous faults affecting the rift margin. Comparison of the Soddo area with adjacent rift sectors (such as the Fonko-Butajira area, where the majority of faults occur within volcano-sedimentary rocks analogous to the Qvs deposits and only a few minor faults affect the Quaternary basalts) suggests the fault-basalt association not to be related to the difference in lithology and erodibility between the Qb and the Qvs rocks but indicates instead a strict relation between basalts and faults. A detailed analysis of the distribution and characteristics of the recent volcanic centers (domes, scoria cones, fissure ridges, etc.) in relation to major and minor faults supports the strong link between the two processes (Figures 11 and 12). In particular, most of the eruptive vents are located along the sigmoidal, *en-echelon* faults that characterize the area between Lake Abaya and the Duguna volcano (Figures 11 and 12). The majority of these centers are represented by basaltic spatter cones (Qb2), although clear relations between faults and volcanoes are also observed for the rhyolitic centers of Salewa Dore and Hako (Qr2–3), whose eruption vents are located along major, roughly NE-SW normal faults (Figure 12). Differently from other MER sectors, where basaltic centers were mostly located at the tips of the faults and open cracks [e.g., in the Northern MER; *Casey et al*., 2006], no preferential location for volcanic centers could be clearly defined either in the field or on satellite imagery (Figure 11). Cones may indeed be located at fault tips, in the center of fault segments or within zones of interactions between faults (such as relay zones; Figure 11); a more limited number of small cones are not apparently strictly related to single faults. The Bilate river volcanic field, north of the Duguna volcano (Figure 2), is the only area where preferential location of spatter cones and tuff rings mostly occurs at the tip of roughly NNE-SSW faults (see supporting information).

[26] In order to better characterize the distribution of vents in the area and to better define their relations with faults, we have mapped vent alignments and assessed their reliability according to the procedure illustrated in *Paulsen and Wilson* [2010]. Vent mapping has been performed on available satellite images (Landsat TM, Aster, Google Earth imagery), digital elevation models (DEMs; SRTM, Aster), and aerial photos. In particular, vent alignments have been mapped on the basis of the spatial distribution of vents as well as their shapes (vent elongation provides a critical parameter to group single vents into an alignment). Reliability of vent alignments has been defined according to parameters such as number of vents, number and characteristics of elongate vents (vents are considered elongate when the ratio between the lengths of the maximum and minimum axes is >1.2), standard deviation from a best fit line, etc. [see *Paulsen and Wilson*, 2010]. The result of this analysis is illustrated in Table 3 and in the graph of Figure 12d, where the azimuthal distribution of elongate vent long axis has also been reported. The distribution of both vent alignments and elongate vent long axis shows a main peak at N20°–25°E, indicating a striking correspondence with the trend of the border faults in the area (compare Figure 12d with Figure 5c) and thus strengthening the close relations between faulting and volcanism. To complete the analysis, we have also calculated the azimuthal distribution of cone breaching, whose results are shown in the graph of Figure 12e. This analysis indicates that the trend of cone breaching tends to parallelize vent alignments (as well as the trend of border faults), with a minor peak orthogonal to this latter trend. Both observations are in agreement with theoretical predictions [*Tibaldi*, 1995].

5. Discussion

5.1. Timing, Architecture, and Kinematics of Deformation in the Soddo Area

[27] The collected data illustrate significant Late Pleistocene-Holocene tectonic activity of the western margin close to Soddo, where radiometric dating of faulted material indicates Late Pleistocene-Holocene (post-30 ka) fault activity. This supports inferences based on analysis of historical seismicity [*Gouin*, 1979; *Keir et al*., 2006], morphotectonic investigations [*Boccaletti et al*., 1998], and recent GPS data [*Kogan et al*., 2012] suggesting active deformation along the western rift margin of the Southern MER. Although not quantifiable because of the lack of subsurface information, deformation is apparently subordinate at the rift axis, where the recent tectono-magmatic activity is likely related to incipient WFB faulting as hypothesized for the Central MER [*Agostini et al*., 2011a]. These findings support models that predict a transition from axial tectono-magmatic deformation in the Northern MER to marginal deformation in the Central and Southern MER, in turn indicating an along-axis, north to south decrease in rift maturity in the MER [e.g., *Hayward and Ebinger*, 1996; *Corti*, 2009; *Agostini et al*., 2011a].

[28] The rift margin at Soddo is characterized by the lack of a major rift escarpment with a gentle transition between the rift floor and the plateau accommodated by numerous faults (Figure 4) with limited lateral extent (maximum length in the range of a few kilometers) and small vertical offset (typically <100 m). This marks a significant difference in margin architecture with respect to the adjacent Fonko-Guraghe and Chencha-Arba Minch areas, where a few large boundary faults with important vertical offset (>1000 m) give rise to prominent fault escarpments. The plan view architecture of the Soddo margin is characterized by a typical array of sigmoidal, right-stepping *en-echelon* normal or oblique faults (Figure 5). Comparison of this architecture with the deformation resulting from analog models of rifting indicates that the fault pattern has been controlled by a sub-E-W (N95°E to N100°E) extension direction, resulting in an oblique extension with respect to the roughly NE-SW-trending rift. This well accords with inversion of fault slip data collected on faults with Pleistocene-Holocene activity, which indicates a N105°E-directed extension (Figure 3), with local variations in the paleostress field likely resulting from stress reorientations and/or influence of volcanic activity [e.g., *Acocella et al*., 2011]. These results are strikingly similar to recent GPS data from the Southern MER [*Kogan et al*., 2012], which also indicate a current N100°E-directed extension at the latitude of Arba Minch (~6°N). Together with our new findings, this suggests that the current Nubia-Somalia relative motion may have acted at least during the Quaternary, consistent with other several geological data from both the Northern and Central MER [e.g., *Boccaletti et al*., 1998; *Wolfenden et al*., 2004; *Bonini et al*., 2005; *Casey et al*., 2006; *Pizzi et al*., 2006; *Agostini et al*., 2011b], plate motion models [e.g., *Jestin et al*., 1994; *Chu and Gordon*, 1999; *Horner-Johnson et al*., 2007], and analog modeling results [*Corti*, 2008; *Agostini et al*., 2011a].

5.2. Relations Between Faulting and Volcanism

[29] Our data support a close correlation between the recent volcanic activity and deformation in the study area, as also suggested by previous works [e.g., *Boccaletti et al*., 1998]. Eruptive vents, mostly represented by basaltic spatter cones with subordinate rhyolitic centers, are located along the recent sigmoidal, *en-echelon* border faults; as a consequence, the trend of vent alignments closely follows that of border faults. Since volcanic alignments provide an indirect means to assess the trend of subsurface dikes [e.g., *Paulsen and Wilson*, 2010, and references therein], the above observations indicate a strong link between boundary faults and the feeder dike system and suggest extension to be accommodated by a combination of faulting and magma intrusion [e.g., *Rooney et al*., 2011]. These characteristics are distinctive of the WFB of the Northern and Central MER, where the strong magma intrusion and magmatic modification of the crust controlled the architecture of deformation and resulted in the array of numerous, small normal faults that are also typical of the Soddo margin. However, despite the similarity in the tectono-magmatic architecture with the WFB, magma geochemistry of the Soddo area is more similar to that found further north along the Silti-Butajira-Debre Zeyt belt, confirming the complexity of the area between latitudes 6.5°N and 7°N, where the two magmatic belts interact and overlap [e.g., *Rooney*, 2010; *Rooney et al*., 2011].

[30] Our statistical analysis indicates that the vent alignments are not orthogonal to the regional extension direction derived from GPS data, fault analysis, and comparison with analog models; rather, since they closely follow the boundary faults, these alignments develop orthogonal to the local

extension direction characterizing the rift margins (see section 4.1). This, together with the observation that analog models suggest the fault pattern to be independent of magmatic processes, indicates that faulting may strongly control magma rising and not vice versa [*Corti*, 2008].

[31] In agreement with *Paulsen and Wilson* [2010], our results support that vent alignments may yield reliable contemporary tectonic stress directions in cases where they are demonstrably young (Quaternary) in age, do not show radial patterns around a polygenetic volcano as is typical for isotropic stress fields, and are not controlled by local factors such as volcano topography, magma chamber shape and pressures, and/or surface loading. However, our data also indicate that these alignments may respond to local stress trajectories (resulting from a reorientation of the extension direction at rift margins) rather than to the regional stress field.

[32] Also, the parallelism between the trend of elongate vent long axes and alignment trends highlighted by our analysis supports that single elongate vents may be independent indicators of subsurface dike trends and may represent independent means for assessing stress directions [*Paulsen and Wilson*, 2010].

6. Conclusions

[33] New geological data provide insights into the distribution, timing, and characteristics of the volcano-tectonic activity on the western margin of the Southern Main Ethiopian Rift in the Soddo area (latitudes between ~7°10'N and ~6°30'N). These new data support the following main conclusions:

[34] 1. C14 radiometric dating of faulted material resulted in ages between ca. 10,900 and 25,300 years B.P., thus pointing to significant Late Pleistocene-Holocene fault activity of the western rift margin close to Soddo. Together with a subordinate deformation at the rift axis, this marginal deformation has been interpreted as reflecting a more immature rifting stage in the Southern MER with respect to the Northern MER, where the tectono-magmatic activity is focused at the rift axis [e.g., *Hayward and Ebinger*, 1996].

[35] 2. Inversion of the fault slip data collected on faults with Pleistocene-Holocene activity, as well as comparison between the fault pattern in the Soddo area and that observed in analog models of low-obliquity rifting, indicates a roughly N100°E extension, in good agreement with recent GPS data from the Southern MER. This suggests that conditions of low-obliquity rifting likely controlled deformation in the area and resulted in the typical sigmoidal, *en-echelon* arrangement of faults observed north of Lake Abaya.

[36] 3. Our data support a close correlation between the recent volcanic activity and deformation in the study area. Statistical analyses of vent alignments and elongate vents show that these trends are not orthogonal to the regional extension direction but closely follow the trend of the recent sigmoidal, *en-echelon* border faults, which form in response to a local stress/strain reorientation.

[37] **Acknowledgments.** We thank Tyrone Rooney, an anonymous reviewer, and the Associate Editor for the detailed comments that helped to improve the manuscript. We also warmly thank Tsegaye Abebe, Samuele Agostini, Ameha Atnafu, Marco Benvenuti, Marco Bonini, Eugenio Carminati, Asfaw Erbello, Tsefaye Kidane, Piero Manetti, and Gezahegn Yirgu for assistance and discussions. G. Corti, M. Philippon, D. Sokoutis, and E. Willingshofer kindly acknowledge the financial support from TOPOMOD, Marie Curie Actions-Networks for Initial Training (ITN), project 264517. G. Corti and F. Sani acknowledge support from the MIUR funds (PRIN2009—prot. 2009H37M59).

References

Abbate, E., and M. Sagri (1980), Volcanites of Ethiopian and Somali Plateaus and major tectonic lines, *Atti Conv. Lincei*, *47*, 219–227.

Abebe, T., P. Manetti, M. Bonini, G. Corti, F. Innocenti, F. Mazzarini, and Z. Pecskay (2005), Geological map (scale 1:200000) of the northern main Ethiopian rift and its implication for the volcano-tectonic evolution of the rift, *Maps Charts Ser., MCH094*, Geol. Soc. of Am., Boulder Colo.

Acocella, V., B. Abebe, and T. Korme (2011), Holocene opening directions along the axes of the Red Sea (Afar) and Main Ethiopian Rifts: An overview, in *Volcanism and Evolution of the African Lithosphere*, edited by L. Beccaluva, G. Bianchini, and M. Wilson, *Spec. Pap. Geol. Soc. Am.*, *478* 25–35, doi:10.1130/2011.2478(02).

Agostini, A., M. Bonini, G. Corti, F. Sani, and F. Mazzarini (2011a), Fault architecture in the Main Ethiopian Rift and comparison with experimental models: implications for rift evolution and Nubia-Somalia kinematics, *Earth Planet. Sci. Lett.*, *301*, 479–492.

Agostini, A., M. Bonini, G. Corti, F. Sani, and P. Manetti (2011b), Distribution of Quaternary deformation in the central Main Ethiopian Rift, East Africa, *Tectonics*, *30*, TC4010, doi:10.1029/2010TC002833.

Angelier, J. (1979), Determination of the mean principal direction of stress for a given fault population, *Tectonophysics*, *56*, T17–T26.

Angelier, J., and P. Mecheler (1977), Sur une méthode graphique de recherché des contraines pricipales également utilisable en tectonique et en sismologie: La méthode des dièdres droits, *Bull. Soc. Geol. Fr.*, *19*, 1309–1318.

Bastow, I. D., S. Pilidou, J.-M. Kendall, and G. W. Stuart (2010), Melt-induced seismic anisotropy and magma assisted rifting in Ethiopia: Evidence from surface waves, *Geochem. Geophys. Geosyst.*, *11*, Q0AB05, doi:10.1029/2010GC003036.

Bendick, R., R. Bilham, L. Asfaw, and S. Klemperer (2006), Distributed Nubia-Somalia relative motion and dyke intrusion in the main Ethiopian rift, *Geophys. J. Int.*, *165*(1), 303–310.

Bigazzi, G., F. P. Bonadonna, G. M. Di Paola, and A. Giuliani (1993), K-Ar and fission-track ages of the last volcano-tectonic phase in the Ethiopian Rift Valley (Tullu Moye area), in *Geology and Mineral Resources of Somalia and Surrounding Regions, Relazi Monogr. Agrarie Subtrop. Trop.*, vol. *113*, edited by E. Abbate, M. Sagri, and F. P. Sassi, pp. 311–322, Ist. Agron. per l'Oltremare, Florence, Italy.

Billham, R., R. Bendick, K. Larson, J. Braun, S. Tesfaye, P. Mohr, and L. Asfaw (1999), Secular and tidal strain across the Ethiopian rift, *Geophys. Res. Lett.*, *27*, 2789–2984.

Boccaletti, M., R. Mazzuoli, M. Bonini, T. Trua, and B. Abebe (1999), Plio-Quaternary volcano-tectonic activity in the northern sector of the Main Ethiopian Rift (MER): relationships with oblique rifting, *Journal of African Earth Sciences*, *29*, 679–698.

Boccaletti, M., M. Bonini, R. Mazzuoli, B. Abebe, L. Piccardi, and L. Tortorici (1998), Quaternary oblique extensional tectonics in the Ethiopian Rift (Horn of Africa), *Tectonophysics*, *287*, 97–116.

Bonini, M., G. Corti, F. Innocenti, P. Manetti, F. Mazzarini, T. Abebe, and Z. Pecskay (2005), Evolution of the Main Ethiopian Rift in the frame of Afar and Kenya rifts propagation, *Tectonics*, *24*, TC1007, doi:10.1029/2004TC001680.

Casey, M., C. J. Ebinger, D. Keir, R. Gloaguen, and F. Mohamad (2006), Strain accommodation in transitional rifts: extension by magma intrusion and faulting in Ethiopian rift magmatic segments, in *The Afar Volcanic Province Within the East African Rift System*, edited by G. Yirgu, C. J. Ebinger, and P. K. H. Maguire, *Geol. Soc. Spec. Publ.*, *259*, 143-163.

Chernet, T. (2011), Geology and hydrothermal resources in the northern Lake Abaya area (Ethiopia), *J. Af. Earth Sci.*, *61*, 129–141.

Chu, D., and R. G. Gordon (1999), Evidence for motion between Nubia and Somalia along the Southwest Indian Ridge, *Nature*, *398*, 64–67.

Corti, G. (2008), Control of rift obliquity on the evolution and segmentation of the main Ethiopian rift, *Nat. Geosci.*, *1*, 258–262.

Corti, G. (2009), Continental rift evolution: from rift initiation to incipient break-up in the Main Ethiopian Rift, East Africa, *Earth Sci. Rev.*, *96*, 1–53.

Corti, G., M. Philippon, F. Sani, D. Keir, and T. Kidane (2013), Re-orientation of the extension direction and pure extensional faulting at oblique rift margins: Comparison between the Main Ethiopian Rift and laboratory experiments, *Terra Nova*, doi:10.1111/ter.12049.

D'Elia, M., L. Calcagnile, G. Quarta, V. Rizzo, C. Sanapo, V. Laudisa, U. Toma, and V. Rizzo (2004), Sample preparation and blank values at the AMS radiocarbon facility of the University of Lecce, *Nucl. Instrum. Methods Res., Sect. B*, *223-224*, 278–283.

de la Torre, I., A. Benito-Calvo, R. Mora, J. Martinez-Moreno, N. Moran, and D. Tibebu (2007), Stone Age occurrences in the western bank of the Bilate River (Southern Ethiopia) – Some preliminary results, *Nyame Akuma*, *67*, 14–25.

Dugda, M. T., A. A. Nyblade, J. Jordi, C. A. Langston, C. J. Ammon, and S. Simiyu (2005), Crustal structure in Ethiopia and Kenya from receiver function analysis: Implications for rift development in Eastern Africa, *J. Geophys. Res.*, *110*, B01303, doi:10.1029/2004JB003065.

Ebinger, C. (2005), Continental breakup: The East African perspective, *Astron. Geophys.*, *46*, 2.16–2.21.

Ebinger, C. J., and M. Casey (2001), Continental breakup in magmatic provinces: An Ethiopian example, *Geology*, *29*, 527–530.

Ebinger, C. J., T. Yemane, G. WoldeGabriel, J. L. Aronson, and R. C. Walter (1993), Late Eocene-Recent volcanism and faulting in the southern main Ethiopian rift, *J. Geol. Soc. London*, *150*, 99–108.

Ethiopian Mapping Agency (1981), *Geological Map of the Ethiopian Rift (scale 1:500.000)*, edited by V. Kazmin, and S. M. Berhe, Ethiopian Mapping Agency, Addis Ababa, Ethiopia.

George, R. M., and N. W. Rogers (1999), The petrogenesis of Plio-Pleistocene alkaline volcanic rocks from the Tosa Sucha region, Arba Minch, southern Main Ethiopian Rift, *Acta Vulcanol.*, *11*, 121–130.

Gibson, I. L. (1969), The structure and volcanic geology of an axial portion of the Main Ethiopian Rift, *Tectonophysics*, *8*, 561–565.

Gouin, P. (1979), *Earthquake history of Ethiopia and the Horn of Africa*, 258 pp., Int. Dev. Res. Cent., Ottawa.

Hayward, N. J., and C. J. Ebinger (1996), Variations in the along-axis segmentation of the Afar Rift system, *Tectonics*, *15*, 244–257.

Horner-Johnson, B. C., R. G. Gordon, and D. F. Argus (2007), Plate kinematic evidence for the existence of a distinct plate between the Nubian and Somalian plates along the Southwest Indian Ridge, *J. Geophys. Res.*, *112*, B05418, doi:10.1029/2006JB004519.

Jestin, F., P. Huchon, and M. Gaulier (1994), The Somalia plate and the East African Rift System: present-day kinematics, *Geophys. J. Inter.*, *116*, 637–654.

Keir, D., C. J. Ebinger, G. W. Stuart, E. Daly, and A. Ayele (2006), Strain accommodation by magmatism and faulting as rifting proceeds to breakup: seismicity of the northern Ethiopian rift, *J. Geophys. Res.*, *111*, B05314, doi:10.1029/2005JB003748.

Kendall, J. M., G. W. Stuart, C. J. Ebinger, I. D. Bastow, and D. Keir (2005), Magma assisted rifting in Ethiopia, *Nature*, *433*, 146–148.

Keranen, K., and S. L. Klemperer (2008), Discontinuous and diachronous evolution of the Main Ethiopian Rift: Implications for the development of continental rifts, *Earth Planet. Sci. Lettt.*, *265*, 96–111, doi:10.1016/j.epsl.2007.09.038.

Kogan, L., S. Fisseha, R. Bendick, R. Reilinger, S. McClusky, R. King, and T. Solomon (2012), Lithospheric strength and strain localization in continental extension from observations of the East African Rift, *J. Geophys. Res.*, *117*, doi:10.1029/2011JB008516.

Leopold, L. B., M. G. Wolman, and J. P. Miller (1964), *Fluvial Processes in Geomorphology*, 522 pp., W. H. Freeman, San Francisco.

Mackin, J. H. (1948), Concept of the graded river, *Geol. Soc. Am. Bull.*, *59*, 463–512.

Mazzarini, F., T. Rooney, and I. Isola (2013), The intimate relationship between strain and magmatism: A numerical treatment of clustered monogenetic fields in the Main Ethiopian Rift, *Tectonics*, *32*, 49–64, doi:10.1029/2012TC003146.

Mohr, P. (1962), The Ethiopian Rift System, *Bull. Geophys. Observ., Addis Ababa*, *5*, 33–62.

Mohr, P. (1967), The Ethiopian Rift System, *Bull. Geophys. Observ., Addis Ababa*, *11*, 1–65.

Mohr, P. (1983), Volcanotectonic aspects of the Ethiopian Rift evolution, *Bull. Cent. Rech. Explor, Prod. Elf Aquitaine.*, *7*, 175–189.

Mohr, P., and B. Zanettin (1988), The Ethiopian food basalt province, in *Continental flood basalts*, edited by J. D. Macdougall, pp. 63–110, Kluwer Acad, Dordrecht, The Netherlands.

Paulsen, T. S., and T. J. Wilson (2010), New criteria for systematic mapping and reliability assessment of monogenetic volcanic vent alignments and elongate volcanic vents for crustal stress analyses, *Tectonophysics*, *482*, 16–28.

Pazzaglia, F. J., T. W. Gardner, and D. J. Merritts (1998), Bedrock fluvial incision and longitudinal profile development over geologic time scales determined by fluvial terraces, in *River Over Rock: Fluvial Processes in Bedrock Channels*, *Geophys. Monogr. Ser., vol. 107*, edited by E. Wohl and K. Tinkler, pp. 207–235, AGU, Washington, D. C.

Pizzi, A., M. Coltorti, B. Abebe, L. Disperati, G. Sacchi, and R. Salvini (2006), The Winji fault belt (main Ethiopian Rift): structural and geomorphological constraints and GPS monitoring, in *The Afar Volcanic Province Within the East African Rift System*, edited by G. Yirgu, C. J. Ebinger, and P. K. H. Maguire, *Geol. Soc. Spec. Publ.*, *259*191–207.

Rooney, T. O. (2010), Geochemical evidence of lithospheric thinning in the southern Main Ethiopian Rift, *Lithos*, *117*, 33–48.

Rooney, T., T. Furman, I. Bastow, D. Ayalew, and G. Yirgu (2007), Lithospheric modification during crustal extension in the Main Ethiopian Rift, *J. Geophys. Res.*, *112*, B10201, doi:10.1029/2006JB004916.

Rooney, T. O., I. D. Bastow, and D. Keir (2011), Insights into extensional processes during magma assisted rifting: Evidence from aligned scoria cones and maars, *J. Volcanol. Geotherm. Res.*, *201*, 83–96.

Tibaldi, A. (1995), Morphology of pyroclastic cones and tectonics, *J. Geophys. Res.*, *100*, 24,521–24,535.

WoldeGabriel, G., J. L. Aronson, and R. C. Walter (1990), Geology, geochronology, and rift basin development in the central sector of the Main Ethiopia Rift, *Geol. Soc. Am. Bull.*, *102*, 439–458.

Wolfenden, E., C. Ebinger, G. Yirgu, A. Deino, and D. Ayale (2004), Evolution of the northern Main Ethiopian rift: Birth of a triple junction, *Earth Planet. Sci. Lett.*, *224*, 213–228.

Zanettin, B., E. Justin-Visentin, M. Nicoletti, and C. Petrucciani (1978), Evolution of the Chencha escarpment and the Ganjiuli graben (Lake Abaya) in the southern Ethiopian rift, *N. Jb. Geol. Paläont. Mh.*, *8*, 473–490.